The Role of Reaction Force and Chemical Potential in Characterizing the Mechanism of Double Proton Transfer in the Adenine−Uracil Complex

Bárbara Herrera and Alejandro Toro-Labbé*

Laboratorio de Química Teórica Computacional (QTC), Facultad de Química, Pontificia Universidad Católica de Chile, Casilla 306, Correo 22, Santiago, Chile

Received: September 12, 2006; In Final Form: April 3, 2007

A theoretical study of the intermolecular double proton transfer in the adenine−uracil base pair has been performed to model the double proton transfer in the adenine−thymine dimer. The mechanism is analyzed in terms of the reaction force profile, which indicates that the activation of the transfer occurs via structural rearrangements to bring the interacting molecules close to each other to let the donor and acceptor atoms in the right position to achieve the transfer. It is found that only when the first proton transfer is partially completed does the second proton get activated, thus illustrating the asynchronous nature of the double proton-transfer process in base pair systems.

1. Introduction

The tempting possibility that imino and enol tautomeric forms of DNA bases be involved in the process of mutagenesis due to their ability to form mispairs with canonical basis of DNA has accompanied molecular genetics since its beginning.[1,2] Proton transfers (PT) in DNA base pairs have been hypothesized as a possible source of spontaneous mutations, since rare tautomers that could be formed might disturb the genetic code.[3,4]

Because of the size of the adenine−thymine (AT) and guanine−cytosine base pairs, quite low computational levels of theory have been used in the study of proton-transfer reactions. First, studies reported that single and double proton-transfer reactions were unfavorable,[5−11] and in more recent papers, the energy barriers in double proton transfer were found to be quite high, regardless of whether the mechanism is concerted or stepwise.[12−14] All studies have agreed that the double proton-transfer reaction (2PT) is more favorable than the single proton transfer (1PT) because in the 2PT reaction, the electroneutrality is maintained.[15] In this paper, an analysis of the double proton transfer in the adenine−uracil (AU) base pair is presented; the AU pair is used as a model of the AT base pair because uracil is smaller than thymine but similar enough to produce results that can be taken as a good reference to characterize the 2PT process in the adenine−thymine system.[16]

An important issue in double proton-transfer reactions is the nature of the process: experimental studies have presented evidence for stepwise or concerted mechanisms.[17−23] Whereas most theoretical papers treat this issue on the basis of the analysis of the energy profile only,[12−14,24−27] in this paper, we present evidence for a stepwise mechanism based on consistency in the observed behavior of various independent global and local molecular properties along the reaction coordinate. Our approach consists of using the reaction force profile[28] to define regions along the reaction coordinate where different mechanisms or specific interactions might be operating. The later are identified by monitoring various properties along the reaction coordinate.[28−37] The big picture of the double proton transfer in the adenine-uracil complex will emerge when consistency of the information on the mechanism obtained from the analysis of independent properties is reached.[28,32−34]

Transition states appearing in the 2PT process will be characterized through the Marcus equation,[38,39] which provides insights to rationalize the barrier heights ($\Delta E^{\ddagger}$) in terms of the reaction energy ($\Delta E°$) and the so-called intrinsic barrier height ($\Delta E_{\circ}^{\ddagger}$), the later mainly due to structural reordering on the whole energetic barrier.

Within the frame of conceptual density functional theory (DFT),[40,41] the chemical potential (μ),[40−46] a global electronic property, has been identified as the negative of the electronegativity.[44,45] It measures the tendency of electrons to escape from an equilibrium distribution. In this context, the chemical potential has been quite useful in characterizing electronic transfer processes.[28,29,40−44] Since chemical reactions involve electron-transfer processes, we introduce in this paper the electronic flux, a new descriptor derived from the chemical potential aimed at identifying the regions along the reaction coordinate where electron transfer is occurring.

This article is organized as follows: Section 2 gives the basic definitions of the descriptors used in this study and the conceptual frame to characterize transition states. Section 3 contains the computational details. In Section 4, the results are presented and discussed. Section 5 contains afew concluding remarks.

2. Theoretical Background

2.1. Energy and Force Profiles. A chemical reaction can be characterized through the changes of geometrical parameters in a multidimensional space. This multidimensional motion is condensed onto the intrinsic reaction coordinate IRC (ξ),[47] so that the energy profile along ξ is the result of the calculation following the minimum energy path relating reactants and products. Numerical differentiation of E (ξ) leads to what we have called the reaction force.[28−34,36,37,39]

$$F(\xi) = -\frac{dE}{d\xi} \tag{1}$$

* To whom correspondence should be addressed. E-mail: atola@puc.cl.

10.1021/jp065951z CCC: $37.00
Published on Web 06/13/2007

This is a global property of the reaction that contains information concerning the specific interactions that drive the reaction from reactants to products.[28] The critical points of $F(\xi)$ define regions along ξ in which different kinds of processes might be taking place.[28,33,34] For a generic double well potential energy profile (elementary step), the reaction force presents two critical points along ξ: the force minimum and maximum. These points define regions that can be interpreted as involving preparation of reactant in the reactant region ($\xi_R \leq \xi < \xi_{min}$), transition to product in the transition state region ($\xi_{min} \leq \xi \leq \xi_{max}$), and relaxation of the product species in the product region ($\xi_{max} < \xi \leq \xi_P$). Three reaction regions are therefore identified in a generic double-well potential energy profile: the reactants, transition state, and product regions.[29,33,34] More complex reactions may need the merge of two or more elementary steps, thus giving rise to the definition of more than three reaction regions. This is the case of the double proton transfer in the adenine−uracil complex.

2.2. Characterization of Transition States. In any chemical reaction, the identification and characterization of transition states (ts) and the physical nature of potential barriers are crucial information to complete the picture of the mechanism associated with a chemical process. The energy of the ts can be rationalized through the use of the Marcus equation, in which the energy barrier, $\Delta E^{\ddagger} = E(\mathrm{TS}) - E(\mathrm{R})$, is given by[38]

$$\Delta E^{\ddagger} = \Delta E_{\circ}^{\ddagger} + \frac{1}{2}\Delta E^{\circ} + \frac{(\Delta E^{\circ})^2}{16\Delta E_{\circ}^{\ddagger}} \tag{2}$$

where $\Delta E_{\circ}^{\ddagger}$ is the intrinsic activation energy, and $\Delta E^{\circ} = [E(\mathrm{P}) - E(\mathrm{R})]$ is the reaction energy. Quite useful results in the rationalization of transition states can be achieved through the Marcus equation for chemical reactions in which $\Delta E^{\ddagger} \gg \Delta E^{\circ}$, that is, reactions in which reactants and products are separated by an energy barrier that is significative in both forward and reverse directions.[28,29,31,39,48] When $\Delta E_{\circ}^{\ddagger}$ is determined from the knowledge of $\Delta E^{\ddagger}$ and ΔE° by solving the second degree equation in $\Delta E_{\circ}^{\ddagger}$ obtained from reordering eq 2,[39] it is possible to determine the parameter β that is defined as the Brønsted coefficient.[49]

$$\beta = \left(\frac{\partial \Delta E^{\ddagger}}{\partial \Delta E^{\circ}}\right) \Rightarrow \beta = \frac{1}{2} + \frac{\Delta E^{\circ}}{8\Delta E_{\circ}^{\ddagger}} \tag{3}$$

β is interpreted as the relative position of the ts in a reduced reaction coordinate that goes from 0 (reactants) to 1 (products);[49] the coefficient β can also be understood as a similarity index relating the transition state to reactants and products.[50] When $\Delta E^{\circ} = 0$, then $\beta = 1/2$; $\beta > 1/2$ if $\Delta E^{\circ} > 0$; and $\beta < 1/2$ if $\Delta E^{\circ} < 0$. These qualitative results indicate that the Marcus equation is consistent with the Hammond postulate.[51]

2.3. Chemical Potential and Electronic Flux. The chemical potential arises in the Euler−Lagrange equation of the energy functional of DFT as a Lagrange multiplier to comply with the condition that the electronic density integrates to N, the total number of electrons of the system.[45] For an N-electron system with total energy E and external potential $v(\vec{r})$, the chemical potential, is defined as[45]

$$\mu = \left(\frac{\partial E}{\partial N}\right)_{v(\vec{r})} = -\chi, \tag{4}$$

where χ is the electronegativity.[44,45,52−55] The use of the finite difference approximation and Koopmans theorem leads to the following working expressions for μ,[41,44,45,53]

$$\mu \approx -\frac{1}{2}(I + A) \approx \frac{1}{2}(\epsilon_L + \epsilon_H), \tag{5}$$

where I is the first ionization potential, A is the electron affinity; ϵ_L and ϵ_H are the energies of the lowest unoccupied and highest occupied molecular orbitals, LUMO and HOMO, respectively.

The evolution of the chemical potential along the reaction coordinate is now used to characterize the electron transfer that occurs in the system during a chemical reaction. The underlying principle behind all transport phenomena is the relationship between flux and gradient. The electronic flux associated with a chemical reaction can be defined as

$$J_{\mu}(\xi) = -Q\frac{\mathrm{d}\mu}{\mathrm{d}\xi}, \tag{6}$$

where Q is the transport coefficient. This coefficient can be calculated from the values of activation and reaction energies and chemical potentials.[28] The profile of this new quantity associated with the chemical potential will be quite useful in identifying the regions along the reaction coordinate that are characterized by electronic reordering and transfer, as shown in Section 4.3.

At this point, it is important to stress the fact that the chemical potential calculated through eq 5 using either ionization potentials and electron affinities or frontier's MO energies has been found to be a quite stable property. For different types of chemical reactions, including proton transfers[30] and internal rotations,[56] it has been observed that its shape along a reaction coordinate is pretty much independent of the method of calculation.[30,56,57] In this context, consistency between the information obtained from the chemical potential and energy profiles will validate, at least qualitatively, the results on the proton-transfer mechanism.

3. Computational Details

The double proton transfer in the AU pair has been characterized at the Hartree−Fock (HF) level of theory using the standard 6-311G** basis set (HF/6-311G**) along the intrinsic reaction coordinate ξ expressed in mass-weighted internal coordinates[58] to allow the dynamic of the whole molecule be characterized during the process. Since the IRC procedure defines the minimum energy path from the transition state toward reactants and products, it necessarily involves full geometry optimization at each step along ξ. All calculations were performed using the Gaussian 03 package.[59] The donor−acceptor pairs labeled {D1, A1} and {D2, A2} are shown in Figure 1, which actually shows the whole mechanism for the 2PT reaction. In the first step (R → ts1 → I), an intermediate complex (I) is produced. This intermediate converts into product in the second step I → ts2 → P. Since Hartree−Fock calculations indicate the existence of two transition states, two consecutive IRC procedures were needed to build up the energy profiles that connect each TS with its own reactants and products. Frequency calculations on reactants, transition states, and products were performed to confirm the nature of the corresponding critical point along the reaction path. Using the optimized geometries obtained from the IRC procedure, molecular properties were determined through single point calculations at the same level of theory.

We are, of course, aware of the fact that remaining questions such as solvent effect[27] or proton tunneling[60] might be important

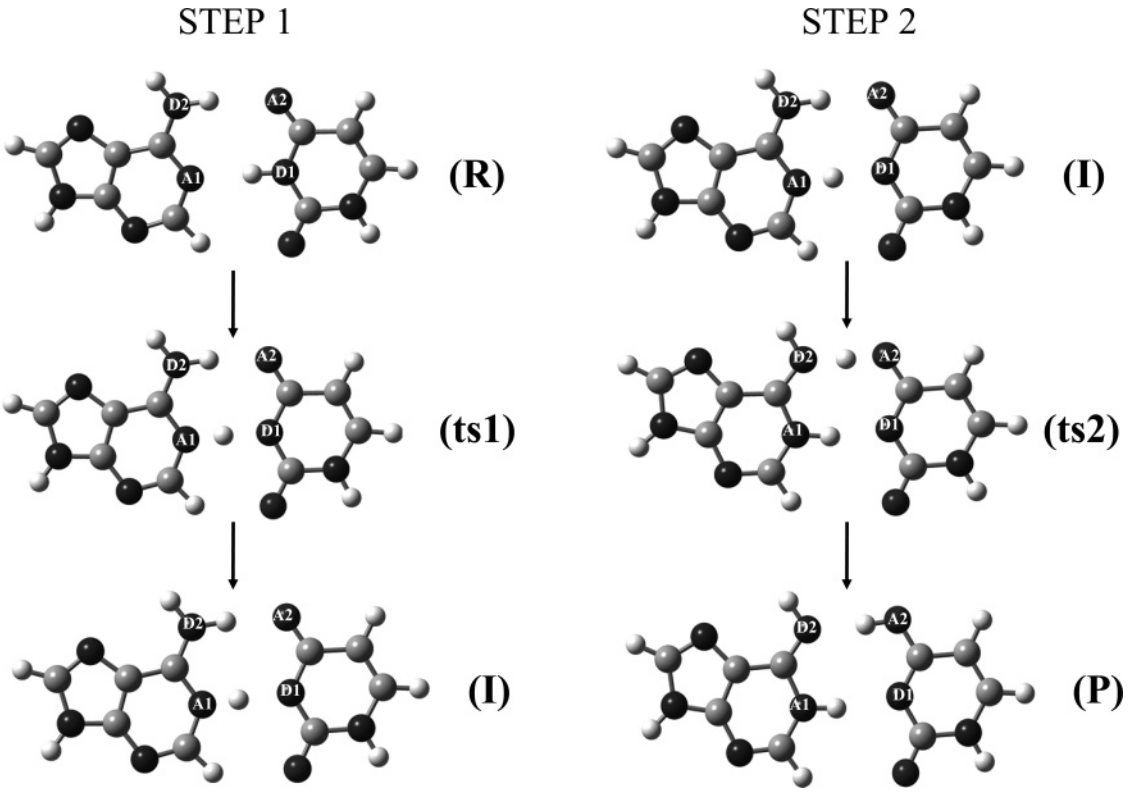

Figure 1. Schematic reaction mechanism for the double proton transfer in the adenine−uracil complex.

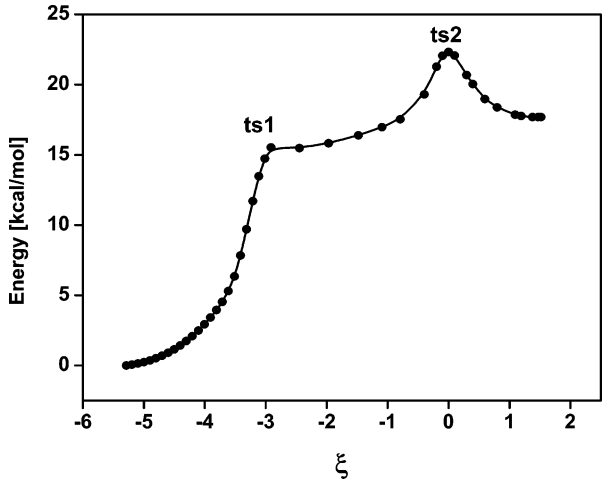

Figure 2. HF/6-311G** energy profiles for the double proton transfer in the adenine−uracil complex.

in some proton-transfer reactions; however, the analysis of these factors is beyond the scope of the current paper.

4. Results and Discussion

4.1. Energetic Parameters and Potential Barriers. In Figure 2 is displayed the HF/6-311G** energy profile along ξ of the double proton transfer in the AU pair. The reaction profile exhibits two maxima with energy barriers $\Delta E_1^{\ddagger} = 15.52$ kcal/mol and $\Delta E_2^{\ddagger} = 6.98$ kcal/mol, the latter measured from the intermediate I, thus indicating the asynchronous nature of the double proton-transfer process. The minimum energy path followed by the protons transferred from donor to acceptor atoms lie in the molecular plane; thus, the C_s symmetry was kept, but not forced, all along the process. Our calculations indicate that as the first proton transfer takes place, the second proton remains bonded to D2 until the first transfer is practically achieved. Once this happens, the second proton detaches from D2 to start its way to A2. This result, backing the stepwise mechanism, is consistent with experimental data of Zewail[21] and Castleman[22] and with theoretical calculations based on more sophisticated methods, including correlation effects.[21,27] Moreover, in a recent paper, Leszczynski et al.[27] have predicted on the basis of B3LYP/6-31G(d) and MP2/6-31G(d) calculations a one-dimensional profile of the total energy change of the adenine−thymine base pair, which is qualitatively similar to that of Figure 2.

Although the Marcus equation cannot be applied to the first transfer because the reaction energy for the R → ts1 → I process is as large as the energy barrier ($\Delta E^{\ddagger} \sim \Delta E^{\circ}$), the intrinsic barrier hindering the second proton transfer can be obtained from eq 2 with $\Delta E_2^{\circ} = [E(\mathrm{P}) - E(\mathrm{I})] = 1.68$ kcal/mol. This gives $\Delta E_{\circ_2}^{\ddagger} = 5.75$ kcal/mol. So according to the Marcus interpretation of eq 2, more than 80% of $\Delta E_2^{\ddagger} = 6.98$ kcal/mol is due to structural reordering; the remaining 1.23 kcal/mol should be associated with electronic effects. Following the TS analysis, the Brønsted coefficient calculated using eq 3 is $\beta_2 = 0.65$, in agreement with the Hammond postulate, which states that endothermic reactions have a productlike transition state so that ts2 resembles more the product of the reaction.[50] On the other hand, since ts1 and the intermediate I are energetically very close, they are expected to be structurally close too. This first indication of the similarity of the pairs {ts1, I} and {ts2, P} will be confirmed later when studying the chemical potential profile.

4.2. The Reaction Force Profile. Owing to the stepwise mechanism of the double proton transfer, there are two transition states along the reaction coordinate, each of them associated with an individual proton transfer. Therefore, the reaction force associated with such an energy profile leads one to identify five reaction regions along ξ. The reactant (R), transition state 1 (TS1), intermediate (I), transition state 2 (TS2), and product

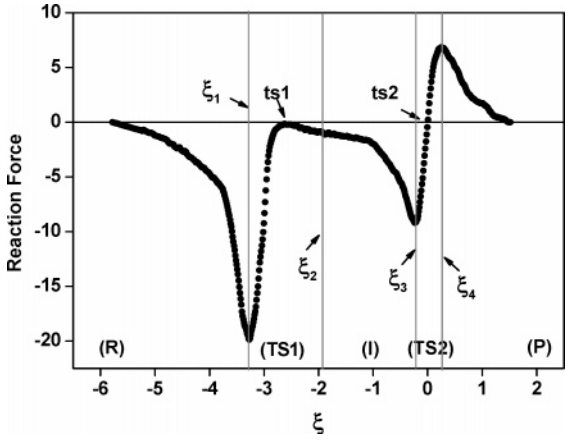

Figure 3. HF/6-311G** reaction force profile (in kcal/mol·ξ) along the reaction coordinate.

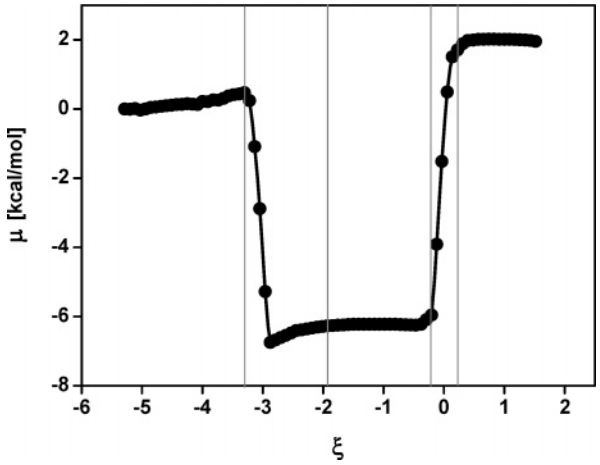

Figure 4. HF/6-311G** chemical potential profile along ξ.

TABLE 1: HF//6-311G Works Involved at the Different Local Processes along ξ for the Double Proton-Transfer Reaction**[a]

work	value
$W_1(R \rightarrow \xi_1)$	11.20
$W_2(\xi_1 \rightarrow ts1)$	4.30
$W_3(ts1 \rightarrow \xi_2)$	0.54
$W_4(\xi_2 \rightarrow \xi_3)$	5.71
$W_5(\xi_3 \rightarrow ts2)$	1.26
$W_6(ts2 \rightarrow \xi_4)$	−1.10
$W_7(\xi_4 \rightarrow P)$	−4.20

[a] All values are in kcal/mol.

(P) regions are indicated in Figure 3. The first step of the reaction is the preparation of reactants through a structural rearrangement that brings the donor and acceptor atoms close to each other to activate the transfer. This requires an amount of energy: $W_1 = -\int_R^{\xi_1} F(\xi)\, d\xi = 11.20$ kcal/mol. The work that follows in the TS1 region is that required to reach the transition state ts1 from ξ_1 (see Figure 2). It is given by $W_2 = -\int_{\xi_1}^{ts1} F(\xi)\, d\xi = 4.30$ kcal/mol. After reaching ts1, there is a small amount of work necessary to launch the activation of the second proton: $W_3 = -\int_{ts1}^{\xi_2} F(\xi)\, d\xi = 0.54$ kcal/mol. Note that the force profile does not exhibit a maximum after ts1 so that ξ_2 is defined arbitrarily in such a way that ts1 is located midway between ξ_1 and ξ_2.

To allow the second proton transfer, an activation work, $W_4 = -\int_{\xi_2}^{\xi_3} F(\xi)\, d\xi = 5.71$ kcal/mol is necessary in order to produce the structural relaxation of the pair {D1, A1} to achieve the first transfer and to bring the couple {D2, A2} as close as possible to each other to facilitate the transfer of the second proton; this is the preparation of the second proton transfer. Note that $W_4 = 5{,}71$ kcal/mol compares very well with the intrinsic barrier $\Delta E_{\circ_2}^{\ddagger} = 5.75$ kcal/mol determined from the Marcus equation. It is worth emphasizing this result because it confirms that the Marcus equation involves a *work* of structural nature.[61,62]

The next step in the second proton transfer needs $W_5 = -\int_{\xi_3}^{ts_2} F(\xi)\, d\xi = 1.26$ kcal/mol to reach the second transition state. It can be noticed that $W_5 < W_4$, thus indicating that structural arrangement that approaches the {D−A} pair needs more energy than the transfer itself, which is accompanied by electronic reordering. The system relaxes, releasing energy, $W_6 = -\int_{ts2}^{\xi_4} F(\xi)\, d\xi = -1.10$ kcal/mol, needed to achieve the second proton transfer and $W_7 = -\int_{\xi_4}^{P} F(\xi)\, d\xi = -4{,}20$ kcal/mol to move away the donor and acceptor moieties in order to complete the relaxation of the product structure. Table 1 summarizes the energy data involved in all the above-mentioned processes.

It is interesting to note that in both transfers, the overall reaction is determined by the preparation steps. These are the structural reordering that brings the donor and acceptor moieties near to each other in order to allow the hydrogen transfer. In other words, both transfers are activated if and only if the donor and acceptor moieties arrange themselves to be in the right position. This process takes a considerable amount of energy (W_1 and W_4). The second hydrogenic motion that starts in the subregion ts1 $\leq \xi \leq \xi_2$, needs less energy ($W_4 < W_1$) due to the assistance of the structural rearrangement that already took place in the reactant region.

4.3. Chemical Potential and Electronic Flux. The profile of μ, calculated from the HOMO and LUMO orbital energies using eq (5), is displayed in Figure 4. It can be noticed that μ remains quite constant along the reactant region, indicating that in this region, mainly the structural reordering is playing a role in the absence of a significative electronic reordering. The chemical potential then drops dramatically at the TS1 region, indicating that in this region, electronic reordering is taking place. Within the intermediate region, μ remains again quite constant at practically the same value as that of ts1, thus indicating that in this region, mainly structural reordering is occurring and confirming, by the way, the similarity of the intermediate complex with ts1. When entering the TS2 region, μ again strongly changes, indicating that the second proton transfer is accompanied by a noticeable electronic reordering. In the product region, μ stabilizes, exhibiting a constant value a little higher than that found at the reactant region. The observed variation of μ along the reaction coordinate is fully consistent with the stepwise mechanism for the double proton transfer in the adeninen-uracil complex; the dramatic variations observed at both transition state regions indicate that strong electronic redistribution is taking place within those regions.

It is important to note that the μ value of ts2 is closer to that of the product species, thus confirming the similarity of the pair {ts2, P} already observed when analyzing the energy profile through the Marcus equation.

Figure 5 displays the evolution of the electronic flux $J_\mu(\xi)$ calculated from eq (6) using $Q = 1$ to characterize the qualitative trend exhibited by the derivative of the chemical potential. It can be observed that the zero flux trend, which is characteristic of equilibrium states, dominates the picture and is only interrupted by two pulses of opposite sign located at the transition state regions as clear signatures of electron reordering

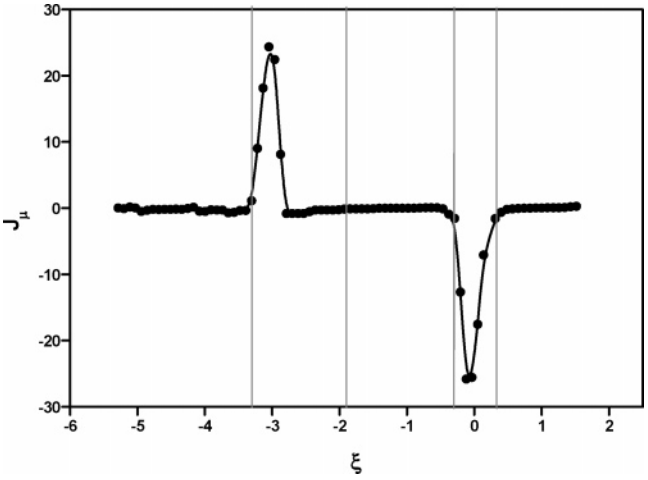

Figure 5. HF/6-311G** electronic flux profile (in kcal/mol·ξ) along ξ. All values in kcal/mol.

regions presenting a nonzero electronic flux. In the reactant, intermediate, and product regions, a zero flux indicates that the electron flow in different directions is exactly balanced. These are regions in which the structural effects overcome the net electronic effects.

So far, the chemical potential and electronic flux profiles are consistent with the energy and reaction force profiles. This result places μ and J_μ as key properties in the characterization of reaction mechanisms; in particular, they are good descriptors of regions along the reaction coordinate where electronic transfer is occurring.

4.4. Electronic Bond Populations. Moving toward the identification of specific interactions that are involved in the charge-transfer process, local electronic properties such as electronic populations associated with bonds that are involved in the proton transfers are analyzed. Figure 6a displays the evolution of Mulliken electronic bond populations of the donor and acceptor atoms with the transferred H (ρ_{D1H1}, ρ_{A1H1}; ρ_{D2H2}, ρ_{A2H2}). The electronic populations within the reactant region remain quite constant, confirming that activation of the first proton transfer needs basically a structural reordering; namely, the approach of the D1 and A1 moieties. At the first transition state region (TS1), ρ_{D1H1} and ρ_{A1H1} populations strongly vary crossing each other. Note that within this region, ρ_{A2H2} and ρ_{D2H2} remain fairly constant, thus indicating that the transfer of the second proton is practically not affected by the first transfer.

At the intermediate region, ρ_{D1H1} and ρ_{A1H1} remain practically unchanged until the formation of the product. This behavior of the electronic populations reflect the electronic reordering taking place within the TS1 region, a result that is consistent with the profiles of chemical potential and electronic flux. On the other hand, it can be observed that the profiles ρ_{D2H2} and ρ_{A2H2} remain fairly constant until the TS2 region is reached, where they change dramatically. This is evidence that the second proton transfer takes place after structural reordering, and it is accompanied by a strong electron reordering, which is induced by the first transfer.

Although the adjacent carbons do not participate directly in the PT process, the analysis of their bond populations helps one to understand the secondary interactions coming out from longer distances.[31,32,34] The bonds formed by the D and A atoms with the adjacent carbon atoms, defines a *backbone* where the proton transfers are localized; the bond populations associated with these bonds are displayed in Figure 6b. The electronic populations on CA and CD change mainly within the TS

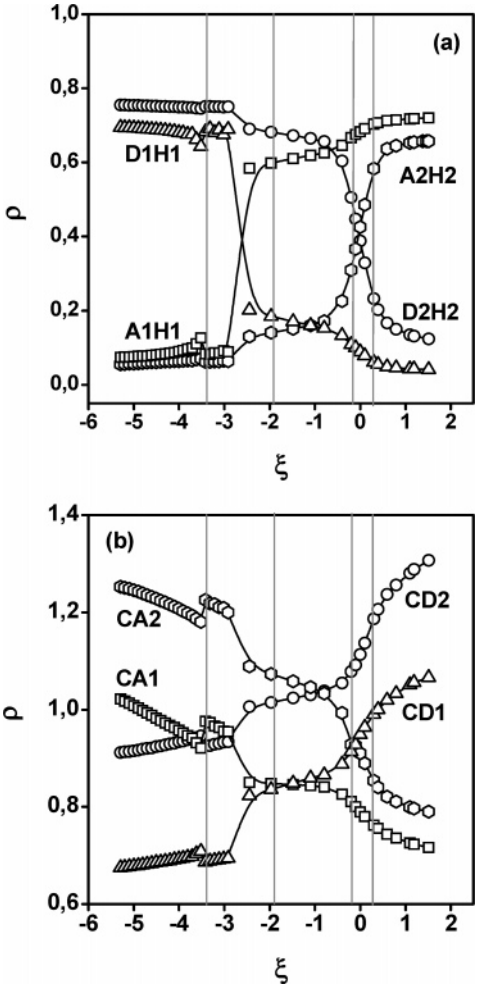

Figure 6. HF/6-311G** Mulliken bond populations involving (a) the transferred hydrogens and (b) the adjacent carbon-donor (ρ_{CD}) and carbon-acceptor (ρ_{CA}) bonds. All values in arbitrary units

regions, indicating that both pyrimidinic and purinic rings reorganize their electronic density in order to compensate for the charge migration evidenced by the μ and J_μ profiles. On the other hand, it is interesting to note that at the reactant and TS1 regions, ρ_{CA1} and ρ_{CD2} are quite close, thus indicating some degree of electronic delocalization. At the intermediate region, these bond populations split to reach the maximum difference at the product. In contrast to this, the ρ_{CA2} and ρ_{CD1} populations are quite different until the TS2 region, where they cross each other, thus indicating a maximum delocalization here.

In summary, the profiles of relevant local electronic populations are consistent with the stepwise mechanism proposed from the analysis of the energy, reaction force, chemical potential, and electronic flux profiles.

5. Concluding Remarks

Although our intention in this work was not to settle the issue of the process's being concerted or stepwise, mainly because the Hartree−Fock procedure does not allow a definitive determination of the variation of the potential energy, the results presented here clearly suggest a stepwise mechanism for the double proton transfer in the adenine−uracil pair. The transfers proceed via structural arrangements of the backbone atoms that promote the first proton transfer, which is accompanied by a delocalization of electronic density. As a response to this electronic reordering, the second transfer is activated. The energy involved in the structural and electronic arrangements has been

quantified in terms of work needed to achieve the different steps of the process. An especially relevant result is that the energy involved in the structural changes necessary to activate the second proton transfer correlates perfectly with the Marcus intrinsic energy barrier[38] that has been for a long time empirically associated with structural effects.

The proton transfers themselves are accompanied by electronic reordering, and the process requires much less energy than the structural changes. Strong electronic flux was detected at the TS regions, whereas an electronic delocalization effect with net zero flux is observed at the reactant, intermediate, and product regions. These results show the chemical potential and the newly defined electronic flux as key properties in characterizing the mechanism of double proton transfer in base pair systems. One important message of this work is that the search for consistency in the behavior of the energy and other global and local properties along a reaction coordinate, within the frame of the reaction force analysis, produces a complete and detailed picture on the mechanisms of chemical reactions.

Acknowledgment. A.T.L. expresses gratitude for a fellowship from the John Simon Guggenheim Foundation (New York). This work was supported by FONDECYT Project No. 1060590, FONDAP Project No. 11980002 (CIMAT), and Proyecto Bicentenario en Ciencias y Tecnología de Inserción en la Academia (PBCT #8).

References and Notes

(1) Watson, J. D.; Crick, F. H. C. *Nature* **1953**, *171*, 964.
(2) Shibata, M.; Zielinski, T. J.; Rein, R. *Theoretical Biochemistry and Molecular Biophysics*; Adenine Press: Guilderland, NY, 1990; Vol. 1.
(3) Jefrey, A.; Saenger, W. *Hydrogen Bonding in Biolgical Systems*; Springer-Verlag: Berlin, 1991.
(4) Steenken, S. *Chem. Biol.* **1997**, *378*, 1293.
(5) Clementi, E.; Mehl, J.; Niessen, W. V. *J. Chem. Phys.* **1971**, *54*, 508.
(6) Clementi, E. *Proc. Natl. Acad. Sci. U.S.A.* **1972**, *69*, 2942.
(7) Kong, Y. S.; John, M. S.; Löwdin, P. O. *Int. J. Quantum Chem., Quantum Biol. Symp.* **1987**, *14*, 189.
(8) Rein, R.; Harris, F. E. *J. Chem. Phys.* **1964**, *41*, 3393.
(9) Lunnel, S.; Sperber, G. *J. Chem. Phys.* **1967**, *46*, 2119.
(10) Scheiner, S.; Kern, C. W. *Chem. Phys. Lett.* **1978**, *57*, 331.
(11) Scheiner, S.; Kern, C. W. *J. Am. Chem. Soc.* **1979**, *101*, 4081.
(12) Hrouda, V.; Florián, J.; Hobsa, P. *J. Phys. Chem.* **1993**, *97*, 1542.
(13) Florián, J.; Hrouda, V.; Hobsa, P. *J. Am. Chem. Soc.* **1994**, *116*, 1457.
(14) Florián, J.; Leszczynski, J. *J. Am. Chem. Soc.* **1996**, *118*, 3010.
(15) Bertrán, J.; Oliva, A.; Rodríguez-Santiago, L.; Sodupe, M. *J. Am. Chem. Soc.* **1998**, *120*, 8159.
(16) Guallar, V.; Duhal, A.; Moreno, M.; Lluch, J. M. *J. Phys. Chem. A* **1999**, *103*, 6251.
(17) Taylor, C. A.; El-Bayoumi, M. A.; Kasha, M. *Proc. Natl. Acad. Sci.* **1969**, *63*, 253.
(18) Jenks, W. P. *Acc. Chem. Res.* **1980**, *13*, 161.
(19) Douhal, A.; Kim, S. K.; Zewail, A. H. *Nature* **1995**, *378*, 260.
(20) Catalán, J.; del Valle, J. C.; Kasha, M. *Proc. Natl. Acad. Sci. U.S.A.* **1999**, *96*, 8338.
(21) Fiebig, T.; Chachisvilis, M.; Manger, M.; Zewail, A.; Douhal, A.; García-Ochoa, I.; de La Hoz, Ayuso, A. *J. Phys. Chem. A* **1999**, *103*, 7419.
(22) Folmer, D.; Wisniewski, E.; Hurley, S.; Castleman, A. *Proc. Natl. Acad. Sci. U.S.A.* **1999**, *96*, 12980.
(23) Sekiya, H.; Sakota, K. *Bull. Chem. Soc. Jpn.* **2006**, *79*, 373.
(24) Catalán, J.; Pérez, P. J. *Theor. Biol.* **1979**, *81*, 213.
(25) Catalán, J.; Palomar, J.; de la Paz, J. L. G. *J. Phys. Chem.* **1997**, *101*, 7941.
(26) Douhal, A.; Guallar, V.; Moreno, M.; Lluch, J. M. *Chem. Phys. Lett.* **1996**, *256*, 370.
(27) Gorb, L.; Podolyan, Y.; Dziekonski, P.; Sokalski, W. A.; Leszczynski, J. *J. Am. Chem. Soc.* **2004**, *126*, 10119.
(28) Toro-Labbé, A. *J. Phys. Chem. A* **1999**, *103*, 4398.
(29) Jaque, P.; Toro-Labbé, A. *J. Phys. Chem. A* **2000**, *104*, 995.
(30) Herrera, B.; Toro-Labbé, A. *J. Phys. Chem. A* **2004**, *108*, 1830.
(31) Herrera, B.; Toro-Labbé, A. *J. Chem. Phys.* **2004**, *121*, 7096.
(32) Toro-Labbé, A.; Gutiérrez-Oliva, S.; Concha, M. C.; Murray, J.; Politzer, P. *J. Chem. Phys.* **2004**, *121*, 4570.
(33) Politzer, P.; Toro-Labbé, A.; Gutiérrez-Oliva, S.; Herrera, B.; Jaque, P.; Concha, M. C.; Murray, J. *J. Chem. Sci.* **2005**, *117*, 467.
(34) Gutiérrez-Oliva, S.; Herrera, B.; Toro-Labbé, A.; Chermette, H. *J. Phys. Chem. A* **2005**, *109*, 1748.
(35) Parra, R.; Dukarevich, I. *J. Chem. Phys.* **2005**, *122*, 144316.
(36) Politzer, P.; Burda, J.; Concha, M.; Lane, P.; Murray, J. *J. Phys. Chem. A* **2006**, *110*, 756. 19
(37) Rincón, E.; Jaque, P.; Toro-Labbé, A. *J. Phys. Chem. A* **2006**, *110*,
(38) Marcus, R. A. *Annu. Rev. Phys. Chem.* **1964**, *15*, 155.
(39) Martínez, J.; Toro-Labbé, A. *Chem. Phys. Lett.* **2004**, *392*, 132.
(40) Parr, R. G.; Yang, W. *Density Functional Theory of Atoms and Molecules*; Oxford University Press: New York, 1989.
(41) Geerlings, P.; Proft, F. D.; Langenaeker, W. *Chem. Rev.* **2003**, *103*, 1793.
(42) Parr, R. G.; Donnelly, R. A.; Palke, W. E. *J. Chem. Phys.* **1978**, *68*, 3801.
(43) Parr, R. G.; Pearson, R. G. *J. Am. Chem. Soc.* **1983**, *105*, 7512.
(44) Pearson, R. G. *J. Am. Chem. Soc.* **1985**, *107*, 6801.
(45) Sen, K. D.; Jorgensen., C. K. *Electronegativity: Structure and Bonding*; Springer-Verlag: Berlin, Germany, 1987; Vol. 66.
(46) Pearson, R. G. *J. Mol. Struct.* (*THEOCHEM*) **1992**, *255*, 261.
(47) Fukui, K. *Acc. Chem. Res.* **1981**, *14*, 363.
(48) Bulat, F.; Toro-Labbé, A. *J. Phys. Chem. A* **2003**, *107*, 3987.
(49) Leffler, J. E. *Science* **1953**, *117*, 340.
(50) Solà, M.; Toro-Labbé, A. *J. Phys. Chem. A* **1999**, *103*, 8847.
(51) Hammond, G. S. *J. Am. Chem. Soc.* **1955**, *77*, 334.
(52) Pauling, L. *The Nature of Chemical Bond*; Cornell University Press: New York, 1960.
(53) Pearson, R. G. *Hard and Soft Acids and Bases*; Dowden, Hutchinson and Ross: Stroudsberg, PA, 1973.
(54) Pearson, R. G. *Coord. Chem. Rev.* **1990**, *100*, 403.
(55) Ayers, P. W.; Parr, R. *J. Am. Chem. Soc.* **2000**, *122*, 2010.
(56) Gutiérrez-Oliva, S.; Letelier, J.; Toro-Labbé, A. *Mol. Phys.* **1999**, *96*, 61.
(57) Zevallos, J.; Toro-Labbé, A. *J. Chil. Chem. Soc.* **2003**, *48*, 39.
(58) González, C.; Schlegel, H. B. *J. Phys. Chem.* **1990**, *94*, 5523.
(59) Frisch, M. J.; Trucks, G. W.; Schlegel, H. B.; Scuseria, G. E.; Robb, M. A.; Cheeseman, J. R.; Montgomery, J. A., Jr.; Vreven, T.; Kudin, K. N.; Burant, J. C.; Millam, J. M.; Iyengar, S. S.; Tomasi, J.; Barone, V.; Mennucci, B.; Cossi, M.; Scalmani, G.; Rega, N.; Petersson, G. A.; Nakatsuji, H.; Hada, M.; Ehara, M.; Toyota, K.; Fukuda, R.; Hasegawa, J.; Ishida, M.; Nakajima, T.; Honda, Y.; Kitao, O.; Nakai, H.; Klene, M.; Li, X.; Knox, J. E.; Hratchian, H. P.; Cross, J. B.; Bakken, V.; Adamo, C.; Jaramillo, J.; Gomperts, R.; Stratmann, R. E.; Yazyev, O.; Austin, A. J.; Cammi, R.; Pomelli, C.; Ochterski, J. W.; Ayala, P. Y.; Morokuma, K.; Voth, G. A.; Salvador, P.; Dannenberg, J. J.; Zakrzewski, V. G.; Dapprich, S.; Daniels, A. D.; Strain, M. C.; Farkas, O.; Malick, D. K.; Rabuck, A. D.; Raghavachari, K.; Foresman, J. B.; Ortiz, J. V.; Cui, Q.; Baboul, A. G.; Clifford, S.; Cioslowski, J.; Stefanov, B. B.; Liu, G.; Liashenko, A.; Piskorz, P.; Komaromi, I.; Martin, R. L.; Fox, D. J.; Keith, T.; Al-Laham, M. A.; Peng, C. Y.; Nanayakkara, A.; Challacombe, M.; Gill, P. M. W.; Johnson, B.; Chen, W.; Wong, M. W.; Gonzalez, C.; Pople, J. A. *Gaussian 03*, revision C.02; Gaussian, Inc.: Wallingford, CT, 2004.
(60) Miura, S.; Tuckerman, M. E.; Klein, M. L. *J. Chem. Phys.* **1998**, *109*, 5290.
(61) Lee, I. H.; Jeung, E. H.; Kreevoy, M. M. *J. Am. Chem. Soc.* **1997**, *119*, 2722.
(62) Lee, I. H.; Jeung, E. H.; Kreevoy, M. M. *J. Am. Chem. Soc.* **2002**, *124*, 7755.